Low-frequency dynamics and medium-range order in vitreous silica

F. Terki, C. Levelut, M. Boissier, and J. Pelous
Laboratoire de Science des Matériaux Vitreux, Université Montpellier II, Place Eugène Bataillon, case 069, 34095 Montpellier Cedex, France
(Received 31 July 1995)

Brillouin and Raman scattering experiments have been performed on vitreous silica samples in order to check the validity of several models proposed for the interpretation of the low-frequency part of the Raman spectrum of glasses including the so-called ''boson peak.'' Samples of various origins, various fictive temperatures, and impurities contents as well as irradiated silica have been considered. It is demonstrated that the softening of acoustic modes responsible for the variation of the location of the boson peak maximum $\omega_{\max}$ is not fully accounted by the variation of the sound velocity V. This indicates that the characteristic length ℓ (related to V and $\omega_{\max}$ in several models) is not a constant. Moreover, a clear quantitative correlation between the hypersound attenuation of the phonons and the low-frequency Raman intensity is evidenced.

I. INTRODUCTION

In the last 20 years most of the discussions concerning the physics of glasses were devoted to the understanding of the low-frequency modes in the range of energies lower than 100 cm^{-1}. In this frequency range the two dominating features are the so-called ''quasielastic light scattering excess'' (QLSE) (below 1 meV=240 GHz=8 cm^{-1}) and the strong broad line around 50 cm^{-1} usually called the ''boson peak'' (BP).

The two-level tunneling systems[1,2] (TLTS's), previously introduced as responsible for the low-temperature behavior of many physical properties, have been extended to help understand the QLSE.[3] However, a very-low-frequency light scattering study in silica at low temperature shows no evidence of a direct relationship between the observed scattered intensity and the TLTS of the glassy state.[4] A generalization to localized entities acting roughly as anharmonic oscillators was next introduced in the soft model approach.[5] Simultaneously, a description in terms of relaxational modes was developed mainly in order to explain neutron and inelastic light scattering.[6] At higher energies, in the frequency range (5–100 cm^{-1}) of the boson peak, vibrational modes are dominant. The temperature dependence of the spectra is mainly determined by the Bose factor, which eliminates the trivial temperature dependence. Based on minimal assumptions about the vibrational modes of glasses, the intensity divided by the Bose factor is proportional to the vibrational density of states, $g(\omega)$, and to a coupling coefficient $C(\omega)$.[7] The ''boson peak'' can be related to a maximum in the coupling coefficient or in the vibrational density of states. The first hypothesis[8] has been contradicted by the presence of a maximum in inelastic neutron scattering experiments in the same frequency range.[9] On the other hand several models explained the boson peak as a characteristic frequency of clusters of a size in the 10–20 Å range.[10–12] Other authors associated the BP with a maximum in the vibrational density of states due to the localization of the phonons by disorder through a mechanism of phonon scattering by density fluctuations.[13–15] Most of these models introduce a connection between the boson peak and a structural characteristic length ℓ of the glass:

$$\omega_{\max}=\frac{2\pi AV}{\ell}, \tag{1}$$

where $\omega_{\max}$ is the frequency of the maximum of the BP, V is the sound velocity, and A is a constant, depending on the model, but generally close to 1. In cluster models,[10–12] this characteristic length may be identified with the cluster size and $\omega_{\max}$ is a typical vibrational frequency of the clusters. In Elliot or Klinger[13,16] models where phonons are localized by disorder, ℓ has the meaning of a localization length.

The low-energy contributions of the relative intensities of vibrational and relaxational states are temperature and composition dependent.[17] Most debates also concern the connection between dynamic and structural aspects as the so-called first sharp diffraction peak.[18–20] All these properties concern the medium-range order which is still one of the most challenging problems in glasses. One possible way to induce modifications of the medium-range order without changing the short-range order is to study the effect of preparation conditions for a fixed chemical composition. This allows one to change significantly the physical properties without large chemical variations. For example the influence of the cooling rate can be studied by comparing glasses of the same composition that have been stabilized by heat treatment at different temperatures in the glass transition range. The temperature of stabilization is usually called the ''fictive temperature'' T_f. The influence of impurities has also been recognized as a relevant parameter to explain changes in the physical properties reflected in relaxational and vibrational modes. More recently, glasses obtained from sol-gel processes have been compared with frozen liquids of the same composition.

In this paper, we attempt to discuss the influence of various parameters on silica samples: the chemical preparation, the OH impurity rate, and the fictive temperature. We point out the evolution of the BP position associated with the vibrational contribution and the relative part of the relaxational

process. We also check the prediction of the connection between the QLSE and the mean free path of the acoustical phonons.[3]

II. EXPERIMENT

A. Samples

Samples of vitreous silica of different origins were investigated. Two of them were commercial samples provided by Quartz et Silice, Nemours, France: a fused quartz called ''puropsil'' and a fused silica named ''tetrasil.'' They differ by their OH content: a few ppm (less than 20) for puropsil and about 1000 ppm for tetrasil. The third sample was prepared by densification of a silica aerogel. The sample of initial density 0.3 $g\,cm^{-3}$ was heat treated at about 1100 °C for several hours until its density reaches the value 2.20 $g\,cm^{-3}$ of amorphous silica. This sample has both a different fictive temperature (lower than 1100 °C) compared to the commercial samples (between 1200 and 1300 °C) and a different OH content (around 3000 ppm). In order to reach high-T_g values, we also investigated a fiber of 300 μm in diameter obtained from tetrasil. Finally, we compared these samples to two samples obtained after a fast neutron irradiation of vitreous silica and crystalline quartz. The two samples were irradiated in the SCK-CEN reactor at Mol (Belgium). At sufficiently high neutron doses, irradiated quartz and irradiated silica converge toward a new amorphous final product different from unirradiated silica.[21] The irradiated silica received a neutron dose corresponding to $180\times10^{18}\,cm^{-2}$. This sample has a density of 2.25 $g\,cm^{-3}$ which represents a densification of 2.5% with respect to nonirradiated amorphous silica. The neutron dose of the irradiated quartz is around $100\times10^{18}\,cm^{-2}$; the resulting density is less than 2.30 $g\,cm^{-3}$. This irradiated quartz is nearly fully amorphized: It corresponds to a neutron dose high enough to make irradiated quartz and irradiated silica nearly similar (see Fig. 1 of Ref. 21).

In these samples the coordination numbers of Si atoms, the SiO_4 tetrahedra, and $\widehat{SiOSi}$ bound angles are very similar. Indeed, it has been shown in a previous x-ray scattering study that the building units of silica are unchanged during the whole process of radiation damage while only the mutual arrangement of these units is modified.[22] Moreover, the Raman and IR spectra of the sol-gel sample in the 500–4000 cm^{-1} frequency range coincide to a large extent with those of vitreous silica except for some weak OH and Si-OH stretching modes.[23–25] As the vibrational modes in this frequency range involve small groups of atoms, this emphasizes large similarities at short-range order.

B. Measurements

The Brillouin scattering measurements of transverse and longitudinal sound velocities at hypersonic frequencies were performed using a high-resolution Fabry-Pérot (FP) spectrometer. The incident light was the 514.5 nm line of a single-mode argon-ion laser (Spectraphysics 2020). The incident power on the sample was about 1 W. A double-passed plane FP spectrometer, whose free spectral range is equal to 75 GHz and finesse equal to 40, is used as a monochromator. The frequency corresponding to the maximum transmission of this filter is matched with the frequency of the Brillouin line by air-pressure adjustment. The resolving unit is a spherical FP interferometer with a free spectral range of 1.48 GHz and a finesse of 50. The total contrast is about 10^7. The accuracy of the experimental data for the sound velocity and the attenuation is, respectively, about 0.1% and 5%. The measurements of the longitudinal sound wave velocity and attenuation are performed in backscattering geometry while the determination of the transverse velocity is obtained in right-angle geometry. In this latter configuration the aperture of the collection lens leads to a significant broadening of the Brillouin line, so that the transverse attenuation cannot be measured accurately.

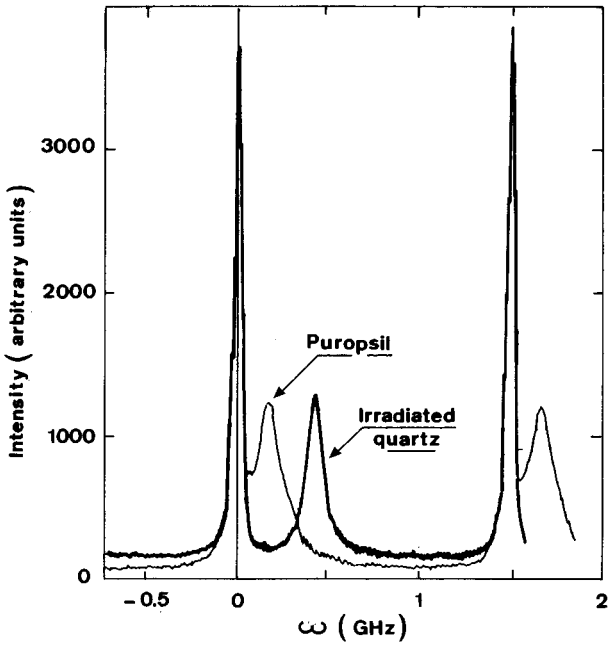

FIG. 1. Example of Brillouin spectra obtained with the high-resolution spectrometer (using the confocal Fabry-Pérot étalon). The Brillouin shift ν_B is related to the apparent Brillouin shift $\delta\nu_B$ by $\nu_B=\delta\nu_B+m\Delta\nu$ where $\Delta\nu$ is the free spectral range of the confocal étalon and m is an integer equal to the difference between the order of interference of the Rayleigh line and the one of the Brillouin line.

Stokes and anti-Stokes Raman spectra were measured in right angle geometry using the same laser line and a conventional triple-pass grating spectrometer (Coderg T800). The resolution is about 1 cm^{-1}. The spectra were recorded in the 5–1500 cm^{-1} frequency range, in both vertical-vertical (VV) and vertical-horizontal (VH) polarizations.

III. RESULTS AND DISCUSSION

A. Brillouin measurements

Two examples of Brillouin spectra recorded using the high-resolution instrument are plotted in Fig. 1. One can note the low width of the Brillouin line for the irradiated quartz. The position and width of the Brillouin line are determined by fitting with the convolution of a Lorentzian function by the experimentally determined apparatus function. The hy-

TABLE I. Hypersonic velocity and attenuation deduced from the fitting procedure performed on the Brillouin data. The position of the maximum of the boson peak, $\omega_{\max}$, is obtained by fitting the VH polarized Raman spectra with a "generalized Lorentzian" for the vibrational contribution. The values of the characteristic length ℓ are deduced from Eq. (1) using the Debye sound velocity (see text). Errors correspond to the upper and lower limits of the 90% confidence interval deduced from the fitting procedure.

Sample	V_L (ms^{-1})	α_L (cm^{-1})	V_T (ms^{-1})	$\omega_{\max}$ (cm^{-1})	ℓ (Å)
Sol-gel silica	5910±10	1950±300	3810±40	52.3±5	26.1±2.5
Tetrasil	5960±10	1800±300	3750±20	58.3±4	23.6±2
Puropsil	5970±10	1550±300	3780±20	58.5±3	23.6±1.5
Fiber	6015±10	-	3900±40	59.2±3	23.5±1.5
Irradiated quartz	6160±10	650±300	3885±20	72.4±5	19.7±2.5
Irradiated silica	6185±10	630±300	-	75±6	19±3

persound transverse and longitudinal velocities are calculated from the Brillouin shift $\delta\nu$ and the refractive index n at 5145 Å:

$$\frac{\Delta\nu}{\nu_0}=2n\left(\frac{V}{c}\right)\sin\frac{\theta}{2}, \tag{2}$$

where V is the sound velocity, c the velocity of light, ν_0 the frequency of the incident light, and θ the scattering angle. The refractive index is taken equal to $n=1.4616$ for all the samples except for the irradiated samples where it is taken equal to $n=1.467$. The hypersound attenuation can be deduced from the Brillouin linewidth Γ as measured in backscattering geometry:

$$\alpha=\frac{4\pi\Gamma}{V}, \tag{3}$$

where α is the hypersonic attenuation, V the sound velocity, and Γ the half width at half maximum of the Brillouin line corrected from the broadening due to the aperture of the collection lens. V is calculated from the Brillouin shift and the refractive index at 5145 Å. The values of transverse and longitudinal hypersonic velocities as well as the attenuation for longitudinal waves are reported in Table I. The results concerning the irradiated silica were previously published in Ref. 21. The two puropsil and tetrasil samples differ mainly by their OH contents. The longitudinal sound velocity is smaller in tetrasil where the OH content is higher. The smaller sound velocity obtained in sol-gel silica also confirms this trend even though sol-gel silica has also a different fictive temperature. Contrary to sound velocity, the hypersonic attenuation seems to increase with increasing OH content. Concerning the influence of the fictive temperature, the sound velocity being higher in tetrasil fiber than in bulk tetrasil, the longitudinal sound velocity seems to increase with increasing fictive temperature. The smaller value for sol-gel silica confirms this variation. Nevertheless, this effect is in contrast with previous work on other glasses.[26,27] This is related to the well-known anomaly in the elastic properties of vitreous silica, which show a small increase with increasing temperature in a broad temperature range. The irradiated quartz and silica show a larger sound velocity and a lower sound wave attenuation than all the other samples. The transverse sound velocity varies like the longitudinal one excepted for the irradiated quartz and the sol-gel silica where the high-resolution analysis of the low transverse signal is obscured by the fluorescence of defects occurring in these two samples. In the fiber, the longitudinal Brillouin line is broadened by index gradient effects so that the attenuation cannot be deduced from the linewidth.

B. Raman measurements

1. Normalization of the data

The first step in analyzing the Raman spectra is to obtain a good superposition of Stokes and anti-Stokes spectra after dividing by the Bose factor over the whole frequency range. We have plotted the reduced intensity defined as

$$I_R(\omega)=\frac{I(\omega)}{\omega(n(\omega,T)+1)} \quad \text{for Stokes Raman intensity,} \tag{4}$$

$$I_R(\omega)=\frac{I(\omega)}{\omega n(\omega,T)} \quad \text{for anti-Stokes Raman spectra,} \tag{5}$$

where $n(\omega,T)$ is the Bose factor. This has been achieved for puropsil, tetrasil, and sol-gel samples by subtracting the noise of the photomultiplier before reduction. However, this subtraction was not sufficient for the tetrasil fiber or the irradiated quartz. In these samples an important frequency-dependent background is superimposed with the Raman scattering. This background is due to a fluorescence signal increasing with frequency which can be attributed to the high rate of defects in the two samples. This contribution has been fitted with a polynomial form and subtracted to the experimental intensity before being reduced by the Bose factor. Then, the treatment of the experimental data yields a good superposition of Stokes and anti-Stokes spectra. Finally, for all the samples the superposition of Stokes and anti-Stokes spectra has been considered to be satisfactory when the ratio of the Stokes intensity to the anti-Stokes intensity is equal to 1 with less than 5% error as can be seen on the example reported in Fig. 2.

The reduced Raman intensities corresponding to various samples were normalized to the integrated intensity in the 120–1000 cm^{-1} frequency range, in which the modes are assumed to be optical modes only. Moreover, we have checked that small changes of the integration boundary do not change the normalization factor.

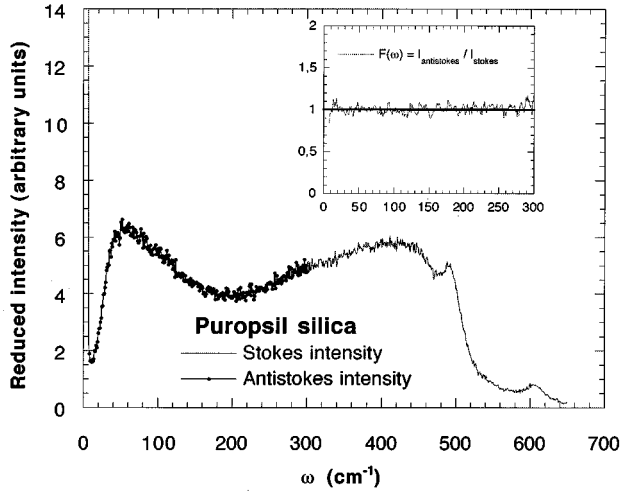

FIG. 2. Example of superposition of Stokes and anti-Stokes low-frequency Raman spectra for puropsil samples in the VV polarization. The inset shows the ratio of the anti-Stokes to the Stokes intensity, equal to 1 within less than 5% error.

2. Defects lines and broad line at 430 cm^{-1}

The reduced intensities for tetrasil, puropsil, and sol-gel samples are plotted in Fig. 3. Very few changes can be noted between puropsil and tetrasil spectra, the only significant difference being a small increase of the so-called $D1$ and $D2$ defect lines[28,29] from puropsil to sol-gel silica. These defect lines have received appreciable attention in the literature. Several interpretations have been proposed, the most recent one being discussed in Ref. 30 where $D1$ is assigned to SiO_4 tetrahedra with a nonbridged oxygen atom and $D2$ is attributed to threefold $(SiO_3)_3$ rings.

The defects lines have small intensities for the sol-gel sample compared to the other ones. This fact is in agreement with previous work showing that the intensities of $D2$ line are expected to increase with increasing fictive

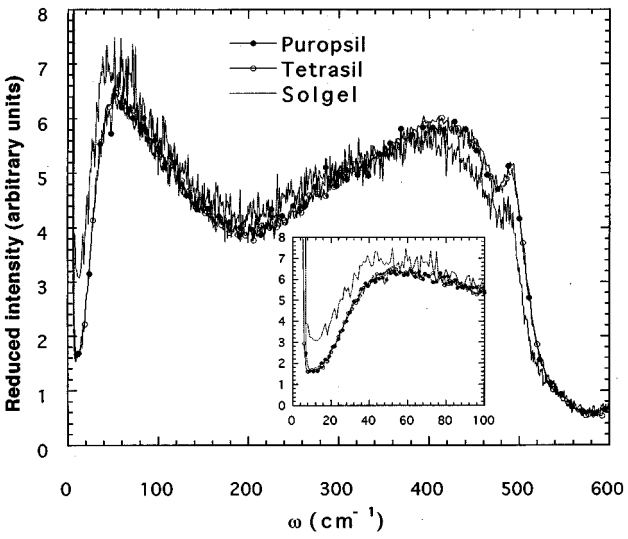

FIG. 3. Comparison of the VV polarized Raman reduced Stokes intensity $I_R(\omega)=I(\omega)/\omega[n(\omega,T)+1]$ for puropsil, tetrasil, and sol-gel silica.

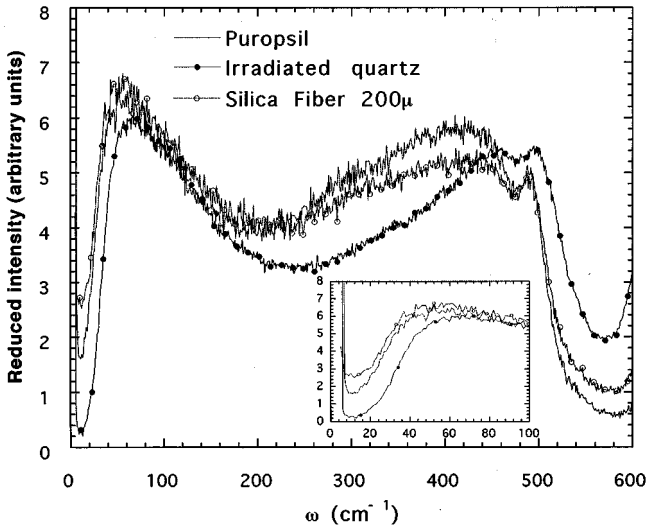

FIG. 4. Comparison of the Raman-reduced Stokes intensity for puropsil, tetrasil fiber, and irradiated quartz in the VV polarization.

temperature.[29,31,32] The reduced intensity of the sol-gel silica is shifted to lower frequencies, indicating a softening of vibrational modes in the whole range of measurements. It is important to emphasize that the decrease of hypersound velocity also reveals a softening for acoustic modes.

In Fig. 4 the tetrasil fiber and the irradiated quartz are compared to the puropsil silica taken as a reference spectrum. We show that these two samples present significant variations of the Raman scattering intensity over the whole frequency range. The differences between these samples are quite important. The intensity of the $D2$ defect line at 600 cm^{-1} is higher for the fiber than for the puropsil, which is also consistent with the work of Galeener.[28] The increase of the defect line intensity occurs at the expense of intensity in the 250–450 cm^{-1} range. This behavior is also associated with a small hardening of modes.[33] The irradiated quartz and silica are characterized by a shift of the dominant line at 430 cm^{-1} toward higher frequencies and a decrease of the width of this broad line. These changes are similar to the effect of high-temperature pressure-induced compaction; for example, a shift of 40 cm^{-1} and a reduction of 50% of the half width at half maximum have been reported for a 5.8% densification.[34] The defect $D2$ line is also strongly enhanced in irradiated quartz compared to unirradiated silica, which agrees with previous work on irradiated silica.[30,35] The intensity of the defect line $D1$ is also expected to increase but to a lesser extent[30] and this variation has not really been observed in our investigation, probably because the induced changes are too small.

3. Depolarization ratio

The depolarization ratio $\rho(\omega)=I_{VH}/I_{VV}$ is plotted in Fig. 5 for puropsil and sol-gel silica in the 10–100 cm^{-1} range. The value $\rho(\omega)$ varies from 0.4 to 0.6 for the various silica samples. The nearly constant (slightly decreasing) value of $\rho(\omega)$ in this frequency range implies that the BP and the quasielastic contributions have the same depolarization ratio as pointed before. This suggests that these two contributions could have some intrinsic relation.

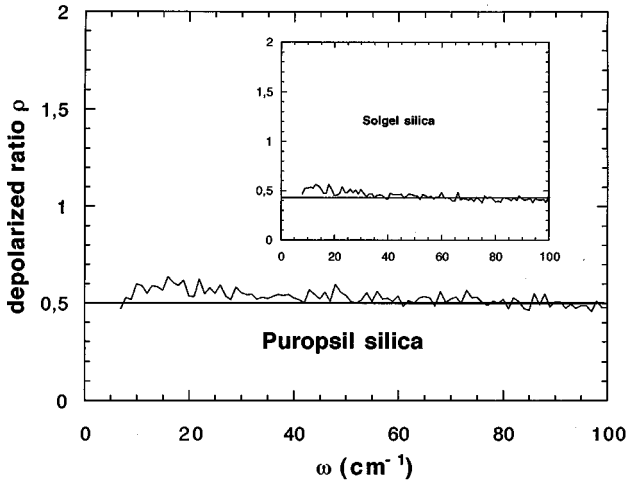

FIG. 5. Comparison of the depolarization ratio $\rho(\omega)$ for two samples of puropsil and sol-gel silica.

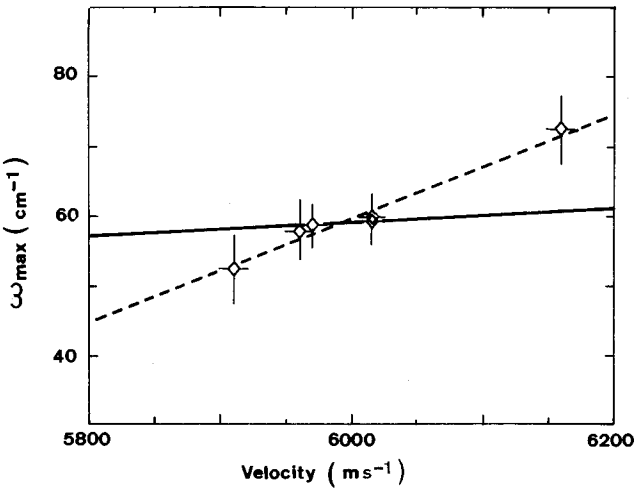

FIG. 6. Variation of the maximum of the boson peak, $\omega_{\max}$, as a function of the sound velocity deduced from Brillouin data. The dashed line represents the best linear regression and the solid line the best linear regression including the origin.

4. Boson peak

In this section, we try to check the validity of various models which have been proposed for the boson peak interpretation. To this purpose, we have carefully determined the position of the maximum of this peak, $\omega_{\max}$, by fitting with several expressions. Then we have correlated these data with hypersonic velocity values deduced from Brillouin scattering.

A fitting procedure is performed on the vibrational contribution of the reduced intensity I_R^{BP} using two different formulas. The first one uses a log-normal expression[37]

$$I_R^{\mathrm{BP}}=\frac{I_0^{\mathrm{BP}}}{(2\pi\sigma^2)^{1/2}}\exp\left(-\frac{(\ln\omega-\ln\omega_{\max})^2}{2\sigma^2}\right), \tag{6}$$

where I_0^{BP} is an amplitude factor, $\omega_{\max}$ is the maximum of the BP, and σ is a parameter related to the width of the BP.

The second ones uses a ''generalized Lorentzian'' expression[38]

$$I_R^{\mathrm{BP}}=I_0^{\mathrm{BP}}\omega^n\frac{1}{[\omega^2+\omega_0^2]^m}, \tag{7}$$

where I_0^{BP} is an amplitude factor, n and m are two exponents, and ω_0 is related to $\omega_{\max}$.

An additional relaxation contribution modeled by a Lorentzian contribution, centered on the laser line, has been taken into account following the ''superposition model.''[38] The vibrational and relaxation contributions are described by independent parameters.

However, another recent work[39,40] takes into account correlations between relaxational and vibrational parts. To analyze the temperature dependence of the spectra the model requires a low-temperature measurement assuming that the relaxational processes are frozen out for this temperature. The authors suggest that the profile of the Rayleigh line wing and its temperature variation can be described within the framework of a model taking into account the quasilocal vibrational excitations responsible for the boson peak. As is pointed out, this model has been developed for temperature-dependent light scattering investigations. But the study of the influence of the temperature is not the purpose of the present work.

The values of $\omega_{\max}$ can be deduced from the fits using formula (6) or (7), with or without a relaxation contribution. We noted that the intensity of the relaxation contribution at room temperature is low so that taking into account the relaxational contribution does not change the value of $\omega_{\max}$ of more than 2 cm^{-1}. The use of Eq. (6) or (7) for the boson peak contribution does not change the value of $\omega_{\max}$ by more than 3 cm^{-1}. The accuracy of $\omega_{\max}$ is quite better using the log-normal expression than Eq. (7) but the frequency range of the fit is shorter. For example, the value of $\omega_{\max}$ deduced from formula (7) with a relaxation contribution is reported in Table I. For the silica samples studied in this paper, the values of $\omega_{\max}$ decrease with decreasing sound velocity.

This effect emphasizes the fact that in most samples $\omega_{\max}$ varies proportionally with the temperature with respect to the sound velocity, i.e., $\ell = V/\omega_{\max} \simeq cste$. This means that the characteristic size is constant with temperature. However, it has been shown that ℓ varies with the fictive temperature.[26] In order to see if a similar effect is observed for small changes (T_f, OH content, . . .) in a given chemical composition sample, we plotted in Fig. 6 the variation of the maximum of the boson peak [using Eq. (7)] with the sound velocity.

We used the Debye sound velocity defined as

$$\frac{3}{V_D^3}=\frac{1}{V_L^3}+\frac{2}{V_T^3}. \tag{8}$$

Due to less accurate values of the transverse sound velocity for fiber and sol-gel samples as discussed in Sec. III A, we used the fact that the experimental ratio V_L/V_T deduced from the other samples is constant. The solid line represents the best linear regression including the origin (corresponding to $\omega_{\max} \propto V$) and the dashed line the linear regression without any constraint. The fit is significantly better in the sec-

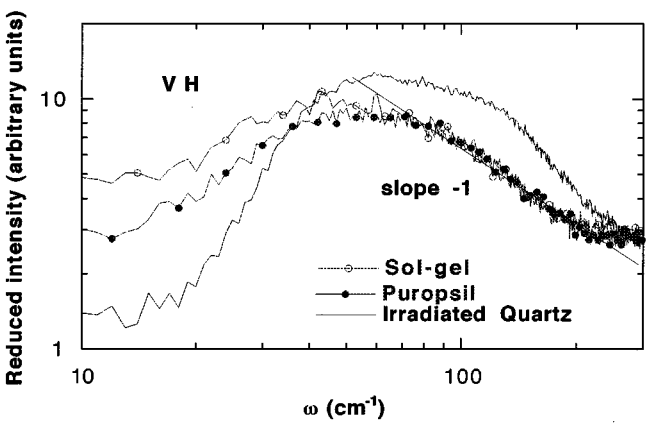

FIG. 7. Reduced intensity versus frequency in log-log scale for three samples in VH polarization. The solid line has been added to show the ω^{-1} behavior ($\omega^{-1.5}$ for the irradiated quartz).

ond case which corresponds to a higher slope, indicating that $\omega_{\max}$ varies faster than the sound velocity. A similar effect has been observed by Buchenau in very fragile glasses (polycarbonates).[36] The values of the characteristic length as defined in Eq. (1) are not constant for all the silica samples. They are calculated using the Debye sound velocity. The decrease of the ℓ value under irradiation has already been observed by Konstantinov *et al.*[35]

Figure 7 shows another important feature. The intensity above the boson peak follows an approximate ω^{-1} behavior represented by the solid line. The reduced intensity is related to the product of the vibrational density of states $g(\omega)$ by the coupling constant $C(\omega)$ through the relation[7]

$$I_R(\omega)=\frac{C(\omega)g(\omega)}{\omega^2}. \tag{9}$$

This behavior of the scattering intensity indicates that the product of $g(\omega)$ by $C(\omega)$ is linear in ω above the boson peak. This ω^{-1} law is observed in VH polarization for all the samples except for the irradiated quartz where other modes seem to be superimposed to the boson peak. The measurements performed in the VV polarization are also disturbed by other contributions (optical modes). A similar ω^{-1} law has already been observed for the dynamical structure factor of neutron data in polymers[36] and in a light scattering investigation performed on a commercial strong glass.[41]

5. Light scattering excess

The first prediction of a correlation between the light scattering excess and the hypersound attenuation was made in 1976 by Theodorakopoulos and Jäckle[3] who describe the excess of Raman intensity observed in silica by Winterling[42] in terms of structural relaxation of defects which can have two distinct states of polarizability. The same defects are responsible for the hypersonic attenuation in a few GHz range. Their paper demonstrates the proportionality of the relaxational Raman scattering excess intensity and the sound wave attenuation which arises from the defect relaxation at the same frequency $\alpha(\omega,T)$:

$$I_{\rm rel}(\omega,T)\propto\frac{1+n(\omega)}{\omega}\alpha_{\rm rel}(\omega,T). \tag{10}$$

Gurevich *et al.*[5] in the framework of the soft-potential model[43] extended this relation to other cases where the Raman intensity and the sound wave attenuation have a common origin. Then the proportionality relationship becomes valid for the total reduced intensity. They also predicted the frequency dependence of the various contributions to the sound wave attenuation. Moreover, they showed that the Raman intensity should also be proportional to the infrared absorption. This has been experimentally observed in a previous work by Stolen[44] in silica. However, the comparison with hypersonic attenuation is still unclear because very few experimental data are available: From Brillouin scattering measurements the attenuation α is extracted only at the frequency of the Brillouin shift (around 1 $\rm cm^{-1}$ for usual glasses). Indeed, few experiments have been performed for this purpose. In the case of silica, the prediction was not really fulfilled except at low temperature.[45] Nevertheless, a rather good agreement versus temperature was found in boron oxide glass.[46] An attempt to extend this comparison to glasses of different composition (B_2O_3-$x$$Li_2O$) Ref. 46 fails because changing significantly the chemical composition induces modifications of the polarizability of the relaxing entities and as a consequence the Raman intensities of the different samples cannot be directly compared. In another work[47] on an optical glass (LaSF7 from Schott), the authors have calculated the Raman intensity from the hypersonic attenuation deduced by using a model of relaxation defects and then compared this calculated intensity to experimental observations. No clear correlation was found. This discrepancy can be explained by the fact that the parameters of the model have been extracted from ultrasonic data; this model did not succeed in reproducing the Brillouin scattering attenuation because defects at hypersonic frequencies introduce additional contributions not efficient at ultrasonic frequencies. For glasses of the same composition with different fictive temperatures,[26] a qualitative agreement is obtained: The Raman scattering intensity and the hypersound attenuation have similar increases with increasing fictive temperatures.

Nevertheless, no quantitative comparison has been performed for several samples. Here we investigate samples with very few changes in the composition (OH content) and we study the influence of the fictive temperature and irradiation. The OH impurities contribute only to some specific high-frequency Raman lines so that the intensities of the different samples are still comparable in a large frequency domain. This is also true for the effect of irradiation or the fictive temperature. Indeed it has also been shown[48] that an increase of the fictive temperature in the 900–1500 °C range induces a modest shift in the frequencies of the host-network vibrational modes and strong changes in the intensity of the two defects modes; on the other hand it has been often mentioned in the literature that the effect of neutron irradiation can be partly explained by a very high fictive temperature. Figure 8 represents the Raman intensity at 10 $\rm cm^{-1}$ as a function of the hypersonic attenuation measured by Brillouin scattering. We plotted both the total Raman-reduced intensity and the relaxational contribution deduced from the Lorentzian part of the fit function described above. As the attenua-

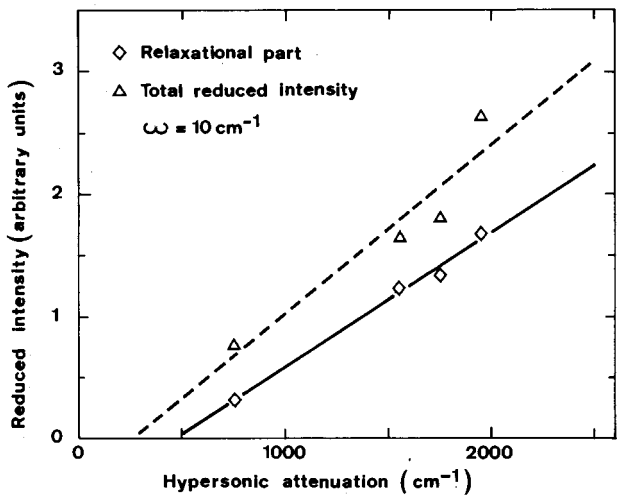

FIG. 8. Total reduced Raman intensity and relaxational contribution to reduced intensity (deduced from the fit using the superposition model) in the VH polarization at 10 cm^{-1} for four silica samples versus hypersonic attenuation measured by Brillouin scattering at about 1 cm^{-1}. The solid and dashed lines are the result of linear regressions.

tion data are obtained at about 1 cm^{-1}, we compared them to the intensity at the lowest frequency available, taking into account the fact that at a frequency lower than 8 cm^{-1} the intensity contains a non-negligible elastic contribution. The correlation between these two physical quantities is rather good, but it is better if one takes only the relaxational contribution of the Raman intensity. In both cases, the result of a linear regression intercepting the attenuation axis at a nonzero value can be explained by contributions to the attenuation due to the scattering of acoustic waves by nonpropagating defects which do not contribute to the quasielastic intensity.

IV. SUMMARY AND CONCLUSION

We have presented a Brillouin and low-frequency Raman scattering investigation on irradiated quartz and silica and of four silica samples which differ by their OH impurity rate or their fictive temperature. These samples had the same chemical composition and very similar short-range order as discussed before in Sec. III B 2. Moreover, defects of the same origin have been observed by ^{29}Si NMR (Ref. 49) in sol-gel silica as well as in vitreous silica, indicating very strong similarities in the short-range order. However, modifications of the medium-range order could be expected. The aim of this study was to test the models proposed for the two dominating features in the low-frequency ($\leqslant 100$ cm^{-1}) Raman spectra: the broad "boson peak" around 50 cm^{-1} and the light scattering excess below 20 cm^{-1}.

In this paper, we have demonstrated that the softening of acoustic modes responsible for the variation of the position of the BP maximum is not fully accounted by the variation of the sound velocity measured by Brillouin scattering. This corresponds to a characteristic length ℓ which is not constant for the six investigated silica samples. The medium-range order in silica samples is modified by changes of the OH content and of the fictive temperature and by neutron irradiation. It is found that ℓ decreases with increasing OH content or fictive temperature and under the effect of neutron irradiation.

On the other hand, several theoretical models predict that the Raman-reduced intensity or its relaxational part should be proportional to the hypersonic attenuation. However, very few experimental proofs of this prediction exist and they concern only one sample as a function of the temperature (B_2O_3) or of the fictive temperature (for barium crown dense glass). We have shown in this paper that there is a clear correlation between the Raman reduced intensity and the hypersonic sound wave attenuation for six different silica samples.

ACKNOWLEDGMENTS

One of the authors (F.T.) is grateful to the Robert Schuman foundation and to the Société de Secours des Amis des Sciences for financial support. The authors also thank Dr. J. P. Bonnet for useful discussions concerning his previous work on irradiated quartz and silica. The authors express their acknowledgments to Dr. T. Woignier for the preparation of a good optical quality sol-gel silica and to Professor R. Jullien for a critical reading of the manuscript.

[1] P. W. Anderson, B. I. Halperin, and C. M. Varma, Philos. Mag. **25**, 1 (1972).
[2] W. A. Phillips, J. Low Temp. Phys. **7**, 351 (1972).
[3] N. Theodorakopoulos and J. Jäckle, Phys. Rev. B **14**, 2637 (1976).
[4] K. B. Lyons, P. A. Fleury, R. H. Stolen, and M.A. Bösch, Phys. Rev. B **26**, 7123 (1982).
[5] V. L. Gurevich, D. A. Parshin, J. Pelous, and H. R. Schober, Phys. Rev. B **48**, 16 318 (1993).
[6] T. Achibat, A. Boukenter, and E. Duval, J. Chem. Phys. **99**, 2046 (1993).
[7] E. Shuker and R. W. Gammon, Phys. Rev. Lett. **25**, 223 (1970).
[8] A. Martin and W. Brenig, Phys. Status Solidi B **64**, 163 (1974).
[9] V. K. Malinovsky, V. N. Novikov, P. P. Parshin, A. P. Sokolov, and M. G. Zemlyanov, Europhys. Lett. **11**, 43 (1990).
[10] T. Pang, Phys. Rev. B **45**, 2490 (1992).
[11] E. Duval, A. Boukenter, and T. Achibat, J. Phys. Condens. Matter **2**, 10 227 (1990).
[12] J. C. Phillips, J. Non-Cryst. Solids **431**, 37 (1981).
[13] S. R. Elliot, Europhys. Lett. **19**, 201 (1992).
[14] E. Akkermans and R. Maynard, Phys. Rev. B **32**, 7850 (1985).
[15] W. Schirmacher and M. Wagener, Solid State Commun. **86**, 597 (1993).
[16] M. I. Klinger, Phys. Lett. A **170**, 222 (1992).
[17] S. L. Isakov, S. N. N. Ishmaev, V. K. Malinovsky, V. N. Novikov, P. P. Parshin, S. N. Popov, A. P. Sokolov, and M. G. Zemlyanov,

Solid State Commun. **86**, 123 (1993).
[18] A. P. Sokolov, A. Kisliuk, M. Soltwisch, and D. Quitmann, Phys. Rev. Lett. **69**, 1540 (1992).
[19] V. N. Novikov and A. P. Sokolov, Solid State Commun. **77**, 243 (1991).
[20] L. Börjesson, A. K. Hassan, J. Swenson, L. M. Torell, and A. Fontana, Phys. Rev. Lett. **70**, 1275 (1993).
[21] J. P. Bonnet, M. Boissier, and A. Ait Gherbi, J. Non-Cryst. Solids **167**, 199 (1994).
[22] R. Comes, M. Lambert, and A. Guinier, in *Proceedings of the Cairo Solid State Conference at the American University in Cairo*, edited by A. Bishay (Plenum, New York, 1967).
[23] A. Bertoluzza, C. Fagnano, M. A. Morelli, V. Gottardi, and M. Guglielmi, J. Non-Cryst. Solids **48**, 117 (1982).
[24] A. Bertoluzza, C. Fagnano, M. A. Morelli, M. Guglielmi, G. Scarinci, and N. Maliavski, J. Raman Spectrosc. **19**, 297 (1988).
[25] V. Gottardi, M. Guglielmi, A. Bertoluzza, C. Fagnano, and M. A. Morelli, J. Non-Cryst. Solids **63**, 71 (1984).
[26] C. Levelut, N. Gaimes, F. Terki, G. Cohen-Solal, J. Pelous, and R. Vacher, Phys. Rev. B **51**, 8606 (1995).
[27] R. Vacher, M. Delsanti, J. Pelous, L. Cecchi, A. Winter, and J. Zarzycki, J. Mater. Sci. **9**, 829 (1982).
[28] F. L. Galeener, J. Non-Cryst. Solids **40**, 527 (1980).
[29] R. A. Barrio, F. L. Galeener, E. Martinez, and R. J. Elliot, Phys. Rev. B **48**, 15 672 (1993).
[30] B. Humbert, A. Burneau, J. P. Callas, and J. C. Lavalley, J. Non-Cryst. Solids **143**, 75 (1992).
[31] These defects lines observed in the Raman spectra have been correlated to ^{29}Si NMR results in silica gels indicating very strong similarities at the short-range order with vitreous silica (Ref. 49).
[32] J. C. Mikkelsen, Jr. and F. L. Galeener, J. Non-Cryst. Solids **37**, 71 (1980).
[33] A. Bouajaj, Ph.D. thesis, Université Claude Bernard, Lyon, 1994.
[34] P. McMillan, B. Piriou, and R. Couty, J. Chem. Phys. **81**, 4234 (1984).
[35] A. V. Konstantinov, L. V. Maksimov, A. R. Silin, and O. V. Yanush, J. Non-Cryst. Solids **123**, 286 (1990).
[36] U. Buchenau, Phys. Rev. Lett. **73**, 2344 (1995).
[37] V. K. Malinovsky, V. N. Novikov, and A. P. Sokolov, Phys. Lett. A **153**, 63 (1991).
[38] M. Krüger, M. Soltwisch, I. Petscherizin, and D. Quitmann, J. Chem. Phys. **96**, 7352 (1992).
[39] V. Z. Gochiyaev, V. K. Malinovsky, V. N. Novikov, and A. P. Sokolov, Philos. Mag. B **63**, 777 (1991).
[40] A. P. Sokolov, A. Kisliuk, D. Quitmann, A. Kudlik, and E. Rössler, J. Non-Cryst. Solids **172-174**, 138 (1994).
[41] F. Terki, J. L. Prat, C. Levelut, M. Boissier, and J. Pelous (unpublished).
[42] G. Winterling, Phys. Rev. B **12**, 2432 (1975).
[43] D. A. Parshin, Phys. Solid State **36**, 991 (1994).
[44] R. H. Stolen, Phys. Chem. Glasses **11**, 83 (1970).
[45] J. Jäckle, in *Amorphous Solids. Low-Temperature Properties*, edited by W. A. Phillips, Topics in Current Physics Vol. 24 (Springer-Verlag, Berlin, 1981).
[46] J. Lörosch, M. Couzi, J. Pelous, R. Vacher, and A. Levasseur, J. Non-Cryst. Solids **69**, 1 (1984).
[47] J. F. Berret, J. Pelous, R. Vacher, A. K. Raychaudhuri, and M. Schmidt, J. Non-Cryst. Solids **87**, 70 (1986).
[48] A. E. Geissberger and F. L. Galeener, Phys. Rev. B **28**, 3266 (1983).
[49] T. Woignier, C. Fernadez-Lorenzo, J. L. Sauvajol, J. F. Schmit, J. Phalippou, and R. Sempere, J. Sol-Gel Sci. Technol. **5**, 1 (1995).